The Canadian Mineralogist
Vol. 54, pp. 899-916 (2016)
DOI: 10.3749/canmin.1500095

COMPLEX Nb-Ta-Ti-Sn OXIDE MINERAL INTERGROWTHS IN THE LA CALANDRIA PEGMATITE, CAÑADA DEL PUERTO, CÓRDOBA, ARGENTINA

MIGUEL ÁNGEL GALLISKI

IANIGLA, CCT-MENDOZA CONICET, Avda. Ruiz Leal s/n, Parque Gral. San Martín; C.C.330 (5500) Mendoza, Argentina

MARÍA FLORENCIA MÁRQUEZ-ZAVALÍA

IANIGLA, CCT-MENDOZA CONICET, Avda. Ruiz Leal s/n, Parque Gral. San Martín; C.C.330 (5500) Mendoza, Argentina
Mineralogía y Petrología, FAD, Universidad Nacional de Cuyo, Centro Universitario (5502), Mendoza, Argentina

PETR ČERNÝ

Department of Geological Sciences, University of Manitoba, Winnipeg, Manitoba R3T 2N2, Canada

RAÚL LIRA

CONICET, Museo de Mineralogía y Geología "Dr. A. Stelzner", F.C.E.F y N., Universidad Nacional de Córdoba. Av. V. Sarsfield 299, (5000) Córdoba, Argentina

ABSTRACT

The assemblage of Nb-Ta-Ti-Sn oxide minerals in some zoned Devonian granitic pegmatites at the La Calandria mine, Cañada del Puerto, shows complex intergrowths of achalaite, ferrotitanowodginite, Ta-rich rutile, columbite-(Mn), ixiolite, and fluorcalciomicrolite. The chemical composition of these phases is variable, but in general the minerals show slight predominance of Nb over Ta and a clearly defined predominance of Fe over Mn, with minor participation of Ti, Sn, and W. The minerals in this assemblage are not in equilibrium and represent magmatic and subsolidus phases that are distinguished texturally and chemically. The primary magmatic stage of mineralization possibly crystallized ixiolite + Ta-rich rutile I in the outer zones of the pegmatite and, less commonly, local columbite-(Mn) in the inner part. Subsolidus unmixing of ixiolite produced achalaite and ferrotitanowodginite I + Ta-rich rutile II. Contemporaneously, Ta-rich rutile I locally exsolved ferrotitanowodginite/achalaite II + cassiterite. A localized Ca-F-rich hydrothermal overprinting event transformed Ta-rich rutile I to Ta-rich rutile III + ferrotitanowodginite/achalaite II + fluorcalciomicrolite. Furthermore, the hydrothermal overprint produced peripheral transformation of columbite-(Mn) to possibly achalaite III and widespread distribution of fluorcalciomicrolite throughout the assemblage.

Keywords: achalaite, ferrotitanowodginite, tantalian rutile, intergrowths, granitic pegmatite, Argentina.

INTRODUCTION

Accessory minerals in granitic pegmatites, especially those that concentrate high field strength elements (HFSE: *e.g.*, W, Zr, Nb, Ta, Ti, Sn, Hf, Th, U), can crystallize in multiple stages under different physico-chemical conditions. The result is a considerable diversity in mineral phases, the study of which can illuminate the behavior of HFSE during the process of pegmatite formation. The evolution of Nb-Ta-Ti-Sn oxide minerals in complex-type rare-element pegmatites, including the petalite, spodumene, lepidolite, and elbaite subtypes and their associated granites, has been investigated in great detail (*e.g.*, Černý *et al*. 1986, Černý & Ercit 1989, Spilde & Shearer 1992, Lumpkin 1998, Novák & Černý 1998, Tindle & Breaks 1998, Tindle *et al*. 1998, Zhang *et al*. 2004, Kontak 2006, Beurlen *et al*. 2007, Van

§ *Corresponding author e-mail address*: galliski@mendoza-conicet.gov.ar

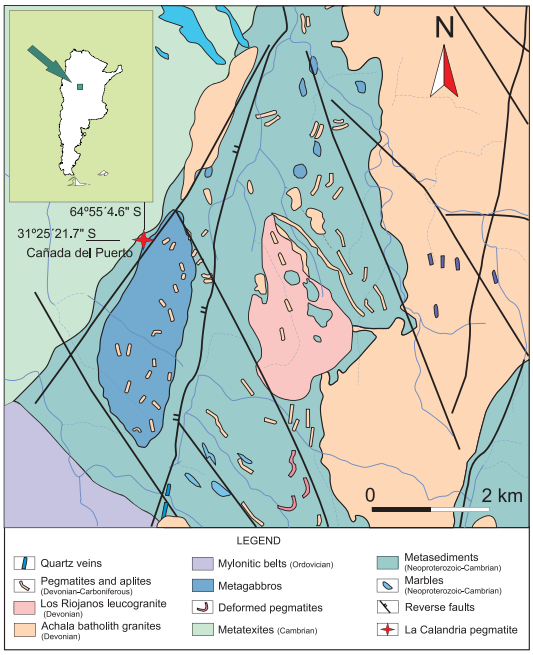

FIG. 1. Location of the La Calandria pegmatites in the geological map of the Cañada del Puerto area (modified from Gaido *et al*. 2005).

Lichtervelde *et al*. 2007, Galliski *et al*. 2008). The geochemically less-evolved beryl-type pegmatites have received less attention (*e.g*., Ercit 1994, Černý *et al*. 1998, Hanson *et al*. 1998, Uher *et al*. 1998a, 1998b, Novák *et al*. 2003, Chudík *et al*. 2011). In this paper, we describe an assemblage of achalaite, Ta-rich rutile, ferrotitanowodginite, columbite-group minerals, and cassiterite that occurs in La Calandria, a rare-element granitic pegmatite of the beryl-columbite-phosphate subtype (Černý & Ercit 2005) in the Sierras Pampeanas, Argentina.

GEOLOGICAL SETTING

Pegmatite and aplite dikes are widespread throughout the western slope of the Sierra Grande de Córdoba, one of several ranges of the Oriental Sierras Pampeanas system of central Argentina. Many of these dikes are concentrated along the central-western margin of the Devonian Achala composite batholith (Lira & Kirschbaum 1990, Demange *et al*. 1996, Dorais *et al*. 1997), which intruded into the Lower Cambrian metasedimentary country rocks of the San Carlos Metamorphic Anatectic Complex (Gordillo 1979, Bonalumi *et al*. 1998 and references therein). About 2 km to the east and northeast of Cañada del Puerto (Fig. 1), the western margin of the batholith is represented mainly by porphyritic and coarse-grained biotite-muscovite monzogranite and muscovite leucogranite of calc-alkaline peraluminous affinity. In this area, gneiss, amphibolite, marble, and locally skarn (Franchini *et al*. 1998) are intercalated with regionally dominant, anatectic, cordierite-garnet-K-feldspar-bearing granitic and tonalitic diatexites.

At Cañada del Puerto, the metamorphic country rocks are mostly biotite-muscovite mylonitic gneiss ("augen gneiss") and subordinate metaquartzite and calc-silicate layers. Locally, the aplite and pegmatite dikes crosscut lens-shaped gabbro bodies which represent minor satellites, tens of meter-sized, of a nearby major intrusion known as the Cañada del Puerto amphibole-bearing metagabbro (Lucero Michaut & Daziano 1984). This gabbro, metamorphosed to amphibolite facies, outcrops as an ellipsoidal body with its major axis oriented NE–SW, ~3000 m long and ~1000 m wide. The smaller satellite bodies, spread over an area of ~20 km^2, are also oriented NE–SW. These lenses were intruded by the Achala granite, which generated retrograde metamorphism of the gabbro and other associated rocks (differentiated gabbroic facies, hornblendite; Bonalumi *et al*. 1998). Their main mineralogy is hornblende (60–70% vol., frequently partially replaced by cummingtonite) and plagioclase (labradorite–bytownite). Drill cores from these mafic rocks also show differentiated interlayered felsic units (1.5–2.5 m thick), classified by Lucero Michaut & Daziano (1984) as anorthosite (>90% bytownite, $An_{70–75}$).

LA CALANDRIA PEGMATITE

At Cañada del Puerto, some of the zoned topaz- and columbite-tantalite-bearing pegmatites (Gay & Lira 1984) host the Nb-Ta-Ti-Sn oxide paragenesis described here. These dikes, located at 31°25′21.7″S, 64°55′4.6″W (northern outcrops) and 31°25′32.5″S, 64°55′47.2″W (southern outcrops), represent a few of a large number of tabular aplites and pegmatites that are exposed on the western slope of the Cerro Los Mogotes (~1800 m a.s.l.) (Fig. 1). As a group, the old surface mining works still recognizable in some dikes are known as La Calandria, where scarce greenish- to pale-blue topaz (misidentified then as beryl) was mined during the 1960s. Because of close similarities in paragenesis and texture, the dikes are considered comagmatic, and the name of the mining works is applied collectively to all of the dikes described here.

In the northern outcrops, three subparallel pegmatite dikes are each separated by ~15–20 m; these dikes outcrop discontinuously along ~250 m of strike length, 0.2–1.5 m in thickness. The pegmatites are concordant with the schistosity of the regional

metasedimentary units, *i.e*., with a strike N25 to 28°E and a dip variable from 20 to 43°W. The southernmost outcrop exposes a 1 m thick pegmatite dike oriented N40°E with an irregular wavy trace and a variable dip that averages 65°W. Dikes in the northern outcrops intrude the metasedimentary gneisses in sharp contact. In contrast, the southernmost La Calandria pegmatites intrude a dark bluish-grey, medium-sized, gabbroic satellite body.

Pegmatites in the northern outcrops are well zoned, often symmetrically. A border zone, 1–2 cm thick, mostly composed of albite with subordinate quartz grains (~1 cm), grades into a coarser-grained (2–2.5 cm) zone, ~3 cm thick, composed of quartz, K-feldspar, albite, and some muscovite. The next, coarser-grained zone includes 1–3 cm-sized topaz crystals (commonly replaced by 2*M*1 yellowish-green muscovite) that grades into a zone richer in K-feldspar and quartz where cm-sized nodules of triplite, some rounded grains of microlite, and 1–2 cm aggregates of dark Nb-Ta oxide minerals are found. In some sectors a quartz core is developed. In the southern outcrops, only chloritization of the amphiboles was noted in the contact zone between the pegmatite and the gabbro. Zoning in the southernmost pegmatite includes a border zone, ~1 cm thick, composed of quartz, plagioclase, and muscovite, followed inwards by an intensely altered assemblage of quartz, plagioclase, and K-feldspar, which is more clearly observed in rocks from the mine dumps than *in situ*. Other mineral species found in this pit are biotite in scarce amounts, topaz, triplite, columbite-group minerals (up to 1 cm crystals, partially altered), and microlite.

Experimental Methods

The minerals investigated are mainly black Nb-Ta-Ti-Sn oxides associated with Qz ± Ab ± Ms ± Brl ± Tpz, most of which are from the intermediate zone of the La Calandria pegmatite. Twelve 3–10 mm-sized samples of the oxide mineral intergrowths were mounted in five compound polished sections and investigated in reflected light with a polarizing microscope and the electron microprobe. The electron-microprobe analyses were carried out in the wavelength-dispersion mode with the Cameca Camebax SX100 equipment at the University of Manitoba with a beam diameter of 2 μm and an acceleration potential of 15 keV. A sample current of 20 nA was measured on Faraday cup, and a counting time of 20 s for each element and 10 s for the backgrounds. The standards used were: microlite (Na*K*α), $MnNb_2Ta_2O_9$ (Ta*M*α), $CaNb_2O_6$ (Ca*K*α), $FeNb_2O_6$ (Fe*K*α), $MnNb_2O_6$ (Mn*K*α, Nb*L*α), orthoclase (K*K*α), rutile (Ti*K*α), stibiotantalite (Sb*L*α), SnO_2 (Sn*L*α), $CaWO_4$ (W*L*α), mimetite (Pb*M*β), $BiTaO_4$ (Bi*M*β), UO_2 (U*M*β), diopside (Si*K*α), $SrBaNb_4O_{10}$ (Sr*L*α), pollucite (Cs*L*α), and $Ba_2NaNb_5O_{12}$ (Ba*L*α), ZrO_2 (Zr*L*α); Na, Cs, Ba, and Sb were sought, but the values obtained were below the detection limits. Data were reduced using the PAP routine of Pouchou & Pichoir (1985). X-ray powder diffraction data were collected using Philips XPERT-PRO PW 3050 equipment at the University of Córdoba. Additional X-ray powder diffraction data were obtained with a Debye-Scherrer camera.

Mineralogy of the Nb-Ta-Ti-Sn Oxides

The Nb-Ta-Ti-Sn oxide minerals in the samples from La Calandria comprise mainly achalaite/ferrotitanowodginite, Ta-rich rutile, columbite-group minerals, cassiterite, and microlite-group minerals; additionally, bismuth forms small inclusions. The chemical compositions of the analyzed samples are plotted in Figures 4, 5, and 6.

Achalaite/ferrotitanowodginite

The precise identification of these minerals at each analyzed point was precluded by the fine-grained intergrowths of several phases. However, X-ray powder diffraction of some samples with simpler phase composition established the presence of a slightly monoclinic phase that would correspond to either achalaite or ferrotitanowodginite, depending on the composition (Galliski *et al*. 2016). The intergrowths that are too fine grained to differentiate by X-ray diffraction of physically separated phases are herein collectively described as "achalaite/ferrotitanowodginite" (Figs. 2–3). These minerals occur in three principal forms: (1) as mm-sized irregular grains with abundant intergrowth of Ta-rich rutile and secondary fluorcalciomicrolite (Fig. 2b–f); (2) as irregular intergrowths of achalaite/ferrotitanowodginite and Ta-rich rutile with probably younger fluorcalciomicrolite (Fig. 2b, c, e); and (3) as very thin rims of ferrotitanowodginite along the contacts of Ta-rich rutile and achalaite (Fig. 3b).

The chemical composition of these minerals is variable (Table 1), but with a slight predominance of Nb over Ta at most of the points and a clearly defined one of Fe over Mn in most of the grains (Fig. 4). The compositions plot in a gap in the Ti-rich ixiolite – Ti-rich columbite field made up of compositions from selected worldwide occurrences (Černý *et al*. 1998), outside the ixiolite field of Černý & Ercit (1989). Titanium is abundant with maximum and average contents of 13.67 and 6.02 wt.% TiO_2, respectively; WO_3, 3.66 and 1.84 wt.%; SnO_2, 7.82 and 2.79 wt.%; and ZrO_2, 1.59 and 0.46 wt.%, respectively. The

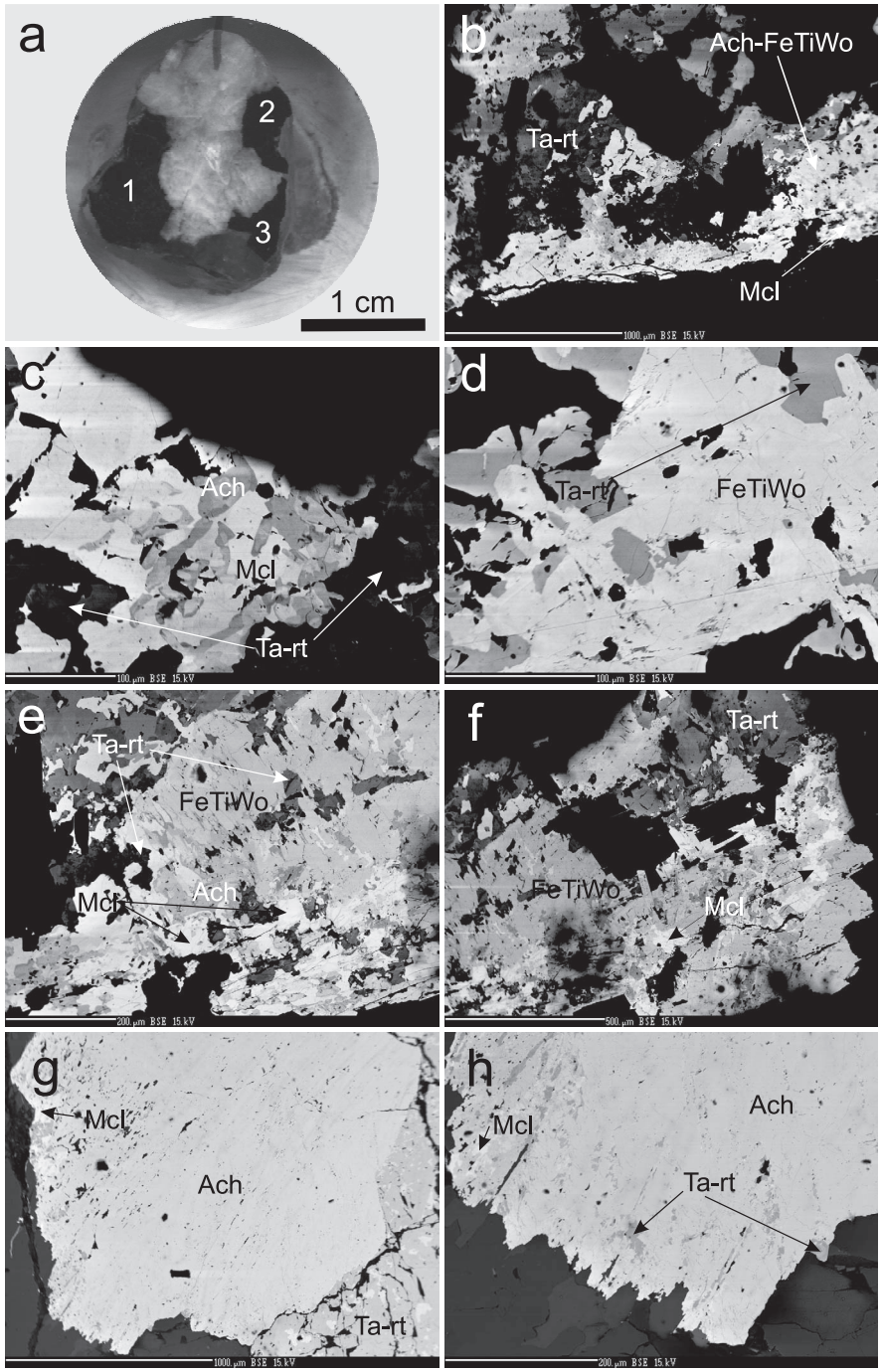

FIG. 2. (a) Polished section (CP1) showing the three analyzed areas in reflected light (CP1-1, -2, -3). Backscattered electron images show the complex intergrowths of achalaite/ferrotitanowodginite, Ta-rich rutile, and microlite. (b) Intergrowths of Ta-rich rutile (Ta-rt), achalaite/ferrotitanowodginite (Ach/FeTiWo), and microlite (Mcl) (CP1-1). (c) Vermiform intergrowths of achalaite (Ach) with variable compositions associated with microlite and Ta-rich rutile (CP1-1). (d) Inclusions of Ta-rich rutile with patchy zoning in ferrotitanowodginite (FeTiWo) (CP1-1). (e) Irregular intergrowths of the

contents of Ti and Sn in the most enriched compositions generally exceed those in the other worldwide occurrences of Ti-rich ixiolite studied by Černý *et al*. (1998), but are in the same range as some of the compositions given by Beurlen *et al*. (2007) for ixiolite from the Borborema pegmatite province in Brazil. In the $(Mn + Fe_T)$–$(Nb + Ta)$–$(W + Ti + Sn + Zr)$ compositional triangle (Fig. 5), our data define a field that lies within the compositional ranges of columbite, wodginite-group minerals, and to a lesser degree, ixiolite, mostly along the 2:1 line, but outside the domains for ixiolite from Prašivá, Slovakia (Uher *et al*. 1998a) and the Borborema pegmatite province, Brazil (Beurlen *et al*. 2007).

Tantalum-rich rutile and fluorcalciomicrolite are associated with or intergrown with achalaite/ferrotitanowodginite. The intergrowths of Ta-rich rutile invariably show higher Ta# than their hosts (Table 1, Figs. 4, 6, 7) and very low Mn#, as expected (Černý *et al*. 1998).

Tantalum-rich rutile

Tantalum-rich rutile is present as mm-sized grains irregularly associated with or as anhedral inclusions in achalaite-ferrotitanowodginite. The largest grains of Ta-rich rutile locally contain irregular inclusions of achalaite or rare intergrowths of cassiterite or ferrotitanowodginite (Fig. 3b). Tantalum-rich rutile is usually irregularly zoned in the largest grains and also in the intergrowths, which occasionally have very thin rims of probable achalaite/ferrotitanowodginite. Less commonly, especially where some crystals have grown along the border of the aggregates of Nb-Ta-Ti-Sn oxide minerals in contact with quartz, they have oscillatory zoning and variable chemical composition, including variable Ti# (Table 2). Titanium contents are high, up to 61.67 wt.% TiO_2. Tantalum is also high, with maximum and average values of 44.97 and 36.45 wt.% Ta_2O_5, respectively; for niobium these values are 22.17 and 10.25 wt.% Nb_2O_5, respectively. Iron, preferentially as Fe_2O_3 and less so as FeO, is also a major component with maximum and averages of 11.61 and 7.09 wt.% and 7.55 and 4.65 wt.%, respectively. Tin is a main component with a maximum of 8.84 wt.% and average of 2.16% SnO_2. Tungsten contents are invariably low with 0.56 wt.% and 0.26% WO_3 maximum and average, respectively. When plotted in the $(Mn + Fe_T)$–$(Nb + Ta)$–$(W + Ti + Sn + Zr)$ triangle, the Ta-rich rutile from La Calandria is more enriched in $(Nb + Ta)$ than at other known occurrences (Fig. 5). In the (Mn#–Ta#) and Ta–$(W + Ti + Sn + Zr)$–Nb diagrams (Figs. 4, 6, 7), almost all of the compositions plot in the field for Ta-rich rutile (except three that correspond to Nb-rich rutile).

Microlite-group minerals

Species of this group are abundant in the fine-grained aggregates as subhedral or, more commonly, irregular or rounded grains that replace achalaite/ferrotitanowodginite or Ta-rich rutile. Several observations suggest that most are secondary in origin: their anhedral form, their increasing abundance in the borders of the Nb-Ta-Ti-Sn oxide minerals where the circulation of post-magmatic Ca-F-rich fluids is easier, and their higher Ta contents relative to the host oxide minerals. In addition, where microlite replaces Ta-rich rutile, Ti preferentially forms secondary Ta-rich rutile with a higher Ti# than its host (see Fig. 3d, where the darkness of the gray color in the BSE image is directly proportional to Ti#), instead of occupying the *B* site of microlite, which is dominantly populated by Ta.

Most of the microlite grains have chemical compositions with Ca dominant and F $>$ 0.5 *apfu* (Table 3) corresponding to fluorcalciomicrolite (see Atencio *et al*. 2010 for definition).

Columbite group minerals

A single grain of columbite-(Mn) (CP4, Fig. 3h) was collected from the inner part of the intermediate zone of the northern pegmatite. Its chemical composition is very depleted in Fe, with low contents of W, Ti, and Sn. In the border of the grain, these elements gradually increase in concentration, culminating in ferrotitanowodginite or achalaite (Fig. 7).

Cassiterite

This mineral was detected only as $\leq$100 μm irregular intergrowths in Ta-rich rutile close to a possible wodginite-group mineral grain. The intergrowths have variable compositions ranging from $>$90 wt.% SnO_2 with $\sim$5 wt.% Fe_2O_3 and other oxides in trace amounts in cassiterite, to SnO_2 values corre-

←

FIG. 2. (continued) four minerals (CP1-1). (f) Ferrotitanowodginite grains growing into interstitial quartz (black), associated with Ta-rich rutile and microlite (CP1-1). (g) A domain with predominant achalaite with intergrowths of Ta-rich rutile (darker grey) and patches of fluorcalciomicrolite, and a second domain to the right consisting of Ta-rich rutile with intergrowths of cassiterite (light grey) and ferrotitanowodginite (CP1-2). (h) Enlarged detail of the complex intergrowths of achalaite, Ta-rich rutile, and microlite shown in (g) (CP1-2).

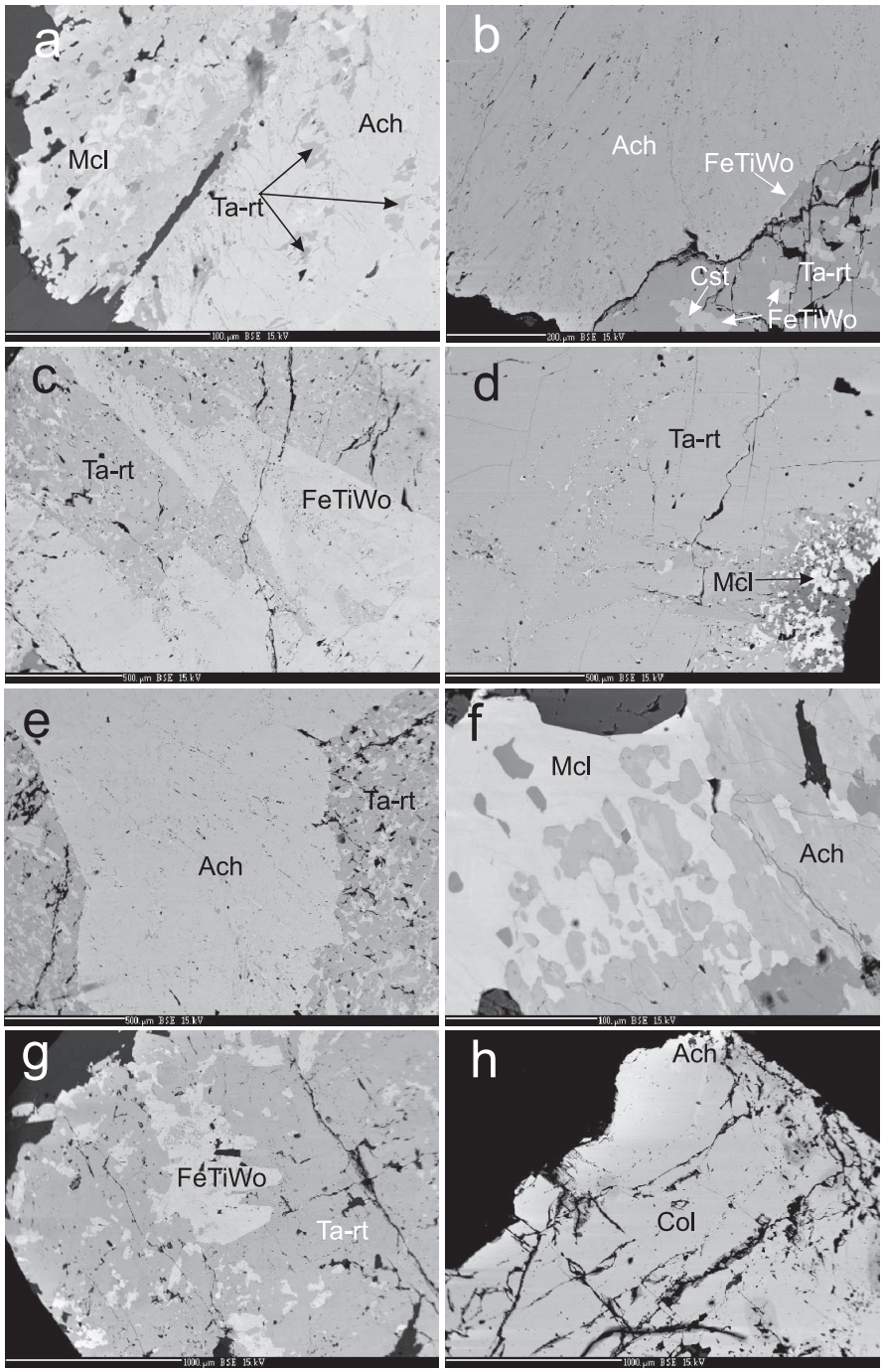

FIG. 3. Backscattered electron images, mineral abbreviations as in Figure 2. (a) Achalaite with intergrowths of Ta-rich rutile and widespread replacement by fluorcalciomicrolite close to the border with quartz (CP1-2). (b) Detail of the domains of achalaite and Ta-rich rutile, respectively, with a rim of ferrotitanowodginite at the interface (CP1-2). (c) Angular crystals of ferrotitanowodginite with small intergrowths of Ta-rich rutile, and Ta-rich rutile with intergrowths of ferrotitanowodginite or achalaite (CP1-2). (d) Tantalum-rich rutile showing some small fissures filled with grains of achalaite/

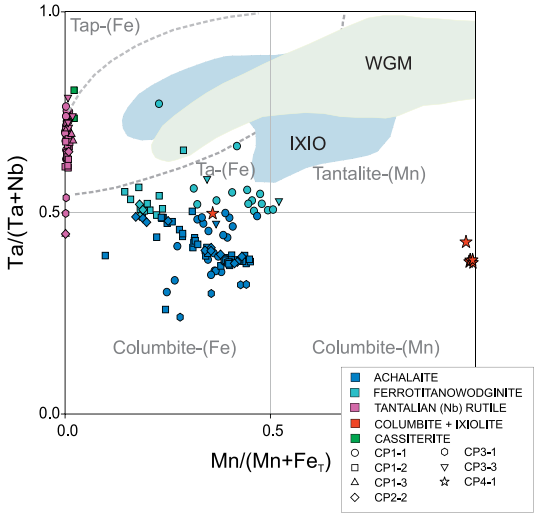

FIG. 4. Chemical compositions of the oxide mineral intergrowths in the La Calandria pegmatite plotted in the columbite quadrilateral. The field (outlined by dashed lines) corresponding to tapiolite-(Fe) [Tap-(Fe)] is taken from Černý *et al*. (1992). The fields labelled WGM and IXIO correspond to wodginite-group minerals and ixiolite, respectively (from Černý & Ercit 1989). The field labelled Ta-(Fe) is that of tantalite-(Fe).

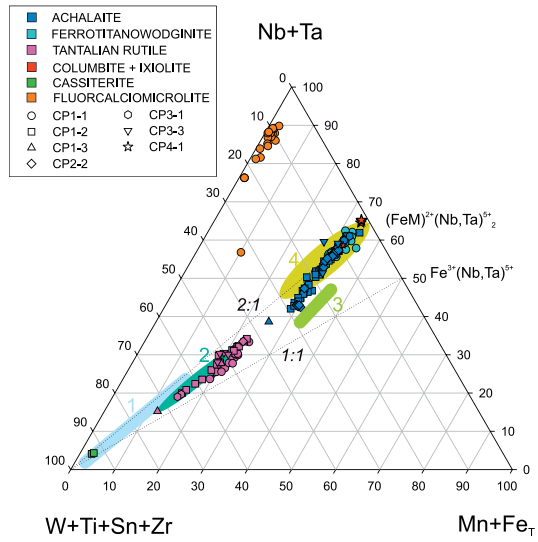

FIG. 5. Compositions of the oxide mineral intergrowths in the La Calandria pegmatite in a (Mn + Fe^{2+} + Fe^{3+})–(Nb + Ta)–(W + Ti + Sn + Zr) diagram. The (Nb + Ta)/(Mn + Fe^{2+} + Fe^{3+}) 2:1 line connects the rutile/cassiterite apex with the ideal composition of the columbite group. Shadowed fields: (1 – light blue) Ta- or Nb-rich rutile from several worldwide occurrences (Černý *et al*. 1998); (2 – turquoise blue) Nb-rich rutile from the Borborema pegmatite province, Brazil (Beurlen *et al*. 2007); (3 – light green) ixiolite from Prašivá, Slovakia (Uher *et al*. 1998a); and (4 – olive yellow) T-rich ixiolite–Ti-rich columbite from various worldwide occurrences (Černý *et al*. 1998).

sponding to those in titanowodginite or ferrotitanowodginite.

Petrographically, along the borders of the Nb-Ta-Ti-Sn oxide mineral intergrowths, irregular grains of Ta-rich rutile or anhedral grains of microlite are somewhat more common, whereas achalaite/ferrotitanowodginite is more abundant in the inner parts.

In detail, the textures between the different phases are varied. The minerals locally occur as grains with rounded borders, irregular shapes, and some vermiform designs (Fig. 2c), or with angular contacts resembling inclusions (Fig. 2d, e). Interpenetrations of achalaite/ferrotitanowodginite with the other phases are also frequent, and occasionally small euhedral prismatic crystals of these phases grew freely in cavities later filled by quartz (Fig. 2f). The achalaite/ferrotitanowodginite groundmass (Fig. 2g, 2h, 3a) includes a very fine intergrowth of micron-sized darker grains of Ta-rich rutile, locally in anhedral crystals, oriented along subparallel cracks (Fig. 2h). Higher magnification reveals achalaite including micron-sized intergrowths of Ta-rich rutile that are usually irregularly zoned, as well as sparser microlite (Fig. 3a). Intergrowths of hosting Ta-rich rutile with angular cassiterite and ferrotitanowodginite also occur, meanwhile at the interface between achalaite and Ta-rich rutile there is a very thin (2–3 μm wide) and irregular rim of ferrotitanowodginite (Fig. 3b). Less frequent are the relationship of ferrotitanowodginite crystals with tiny inclusions of Ta-rich rutile contained in a

←

FIG. 3. (continued) ferrotitanowodginite. A sector in the border zone is locally replaced by microlite; note the associated development of secondary Ta-rich rutile, which has a higher Ti# (CP1-3). (e) Achalaite hosting intergrowths of Ta-rich rutile is associated with Ta-rich rutile with intergrowths of achalaite/ferrotitanowodginite (CP2-1). (f) Achalaite with intergrowths of Ta-rich rutile profusely replaced by fluorcalciomicrolite (CP1-2B). (g) Primary Ta-rich rutile with intergrowths of ferrotitanowodginite (CP3-3). (h) Columbite-(Mn) (Col) transitionally replaced in its border by possible achalaite (Ach) (CP4-1).

TABLE 1. SELECTED CHEMICAL COMPOSITIONS OF MINERALS FROM THE LA CALANDRIA GRANITIC PEGMATITE

Mineral	ACH	ACH	FTW	FTW	ACH	FTW	ACH	ACH	FTW	FTW	ACH	FTW	FTW	ACH
Sample	CP1-1	CP1-1	CP1-1	CP1-1	CP1-2	CP1-2	CP1-2	CP1-2	CP1-2	CP1-2	CP1-2	CP1-2	CP1-2	CP2-2
Point	26	31	33	79	88	97	B-06	B-40	B-42	B-45	B-46	B-53	B-54	B-64
Position	host	host	host	exs.	host	exs.	host	host	exs.	exs.	host	coex.	coex.	coex.
WO_3 wt.%	1.03	0.69	0.83	0.66	2.39	1.25	2.70	2.28	1.70	1.23	3.28	0.62	2.42	2.76
Ta_2O_5	47.03	39.59	45.31	49.38	36.15	44.85	36.73	35.77	42.56	44.81	37.87	42.44	38.90	37.12
Nb_2O_5	28.34	33.27	26.72	23.61	31.87	22.76	35.83	35.56	24.59	26.55	23.99	19.77	21.34	34.70
TiO_2	3.78	5.82	6.46	5.98	6.45	6.95	4.56	4.68	7.00	6.28	8.98	11.71	10.92	4.70
SnO_2	0.99	1.97	1.77	2.10	3.51	6.31	1.64	1.42	5.89	3.63	7.27	5.92	6.39	1.55
ZrO_2	0.00	0.00	0.00	0.00	0.00	0.00	0.49	0.60	0.91	0.72	1.25	1.14	1.59	0.43
UO_2	0.19	0.00	0.91	0.50	0.30	0.06	0.38	0.27	0.12	0.15	0.21	0.18	0.32	0.24
SiO_2	0.42	0.44	0.36	0.50	0.60	0.67	0.06	0.33	0.19	0.22	0.09	0.10	0.11	0.22
Sb_2O_3	0.00	0.00	0.00	0.00	0.00	0.00	0.00	0.00	0.00	0.00	0.00	0.00	0.00	0.00
Bi_2O_3	0.00	0.00	0.00	0.05	0.03	0.00	0.00	0.03	0.08	0.00	0.00	0.03	0.07	0.03
Fe_2O_3	2.05	2.68	1.89	2.30	3.17	3.44	1.75	2.27	4.34	2.64	6.18	7.83	7.71	1.82
FeO	8.22	9.77	6.75	6.63	8.07	8.74	9.00	8.21	8.24	8.66	6.91	5.95	6.06	8.08
MnO	6.35	4.52	7.10	6.84	5.64	3.47	6.61	6.77	3.73	4.89	3.80	2.81	3.21	7.26
PbO	0.11	0.00	0.09	0.00	0.00	0.00	0.02	0.05	0.10	0.00	0.29	0.17	0.07	0.00
CaO	0.01	0.07	0.02	0.01	0.01	0.01	0.00	0.02	0.02	0.03	0.02	0.01	0.02	0.01
SrO	0.01	0.00	0.00	0.00	0.01	0.03	0.00	0.00	0.07	0.00	0.00	0.06	0.00	0.00
TOTAL	98.53	98.82	98.21	98.56	98.20	98.54	99.77	98.26	99.54	99.81	100.14	98.74	99.13	98.92

TABLE 1. CONTINUED.

Mineral	ACH	ACH	FTW	FTW	ACH	FTW	ACH	ACH	FTW	FTW	ACH	FTW	FTW	ACH
Sample	CP1-1	CP1-1	CP1-1	CP1-1	CP1-2	CP1-2	CP1-2	CP1-2	CP1-2	CP1-2	CP1-2	CP1-2	CP1-2	CP2-2
Point	26	31	33	79	88	97	B-06	B-40	B-42	B-45	B-46	B-53	B-54	B-64
Position	host	host	host	exs.	host	exs.	host	host	exs.	exs.	host	coex.	coex.	coex.
W (*apfu*)	0.074	0.047	0.059	0.047	0.163	0.088	0.183	0.156	0.118	0.086	0.221	0.042	0.163	0.189
Ta	3.536	2.828	3.370	3.720	2.581	3.319	2.617	2.565	3.098	3.272	2.678	3.020	2.746	2.666
Nb	3.542	3.951	3.304	2.957	3.783	2.800	4.244	4.239	2.975	3.223	2.821	2.339	2.505	4.144
Ti	0.786	1.150	1.329	1.246	1.274	1.423	0.899	0.928	1.409	1.268	1.757	2.305	2.133	0.934
Sn^{4+}	0.109	0.206	0.193	0.232	0.367	0.685	0.171	0.149	0.628	0.389	0.754	0.618	0.661	0.163
Zr	0.000	0.000	0.000	0.000	0.000	0.000	0.063	0.077	0.119	0.094	0.159	0.145	0.201	0.055
U^{4+}	0.012	0.000	0.055	0.031	0.018	0.004	0.022	0.016	0.007	0.009	0.012	0.010	0.018	0.014
Si	0.116	0.116	0.098	0.139	0.158	0.182	0.016	0.087	0.051	0.059	0.023	0.026	0.029	0.058
Sb	0.000	0.000	0.000	0.000	0.000	0.000	0.000	0.000	0.000	0.000	0.000	0.000	0.000	0.000
Bi	0.000	0.000	0.000	0.004	0.002	0.000	0.000	0.002	0.006	0.000	0.000	0.002	0.005	0.002
Fe^{3+}	0.426	0.529	0.389	0.479	0.625	0.704	0.345	0.449	0.875	0.534	1.209	1.542	1.506	0.363
Fe^{2+}	1.900	2.147	1.544	1.537	1.772	1.988	1.973	1.811	1.845	1.946	1.503	1.303	1.317	1.785
Mn	1.487	1.006	1.645	1.605	1.254	0.800	1.467	1.512	0.846	1.112	0.837	0.623	0.706	1.624
Pb	0.008	0.000	0.007	0.000	0.000	0.000	0.001	0.004	0.007	0.000	0.020	0.012	0.005	0.000
Ca	0.003	0.020	0.006	0.003	0.003	0.003	0.000	0.006	0.006	0.009	0.006	0.003	0.006	0.003
Sr	0.002	0.000	0.000	0.000	0.002	0.005	0.000	0.000	0.011	0.000	0.000	0.009	0.000	0.000
TOTAL	12.001	12.000	11.999	12.000	12.002	12.001	12.001	12.001	12.001	12.001	12.000	11.999	12.001	12.000
Ta#	0.50	0.42	0.50	0.56	0.41	0.54	0.38	0.38	0.51	0.50	0.49	0.56	0.52	0.39
Mn#	0.39	0.27	0.46	0.44	0.34	0.23	0.39	0.40	0.24	0.31	0.24	0.18	0.20	0.43
Ti#	0.10	0.15	0.17	0.16	0.17	0.19	0.12	0.12	0.19	0.16	0.24	0.30	0.29	0.12

Fe_2O_3 and FeO calculated by charge balancing.
ACH = achalaite, FTW = ferrotitanowodginite, incl. = inclusion, exs. = exsolution, coex. = coexisting, all related to Ta-rich rutile.

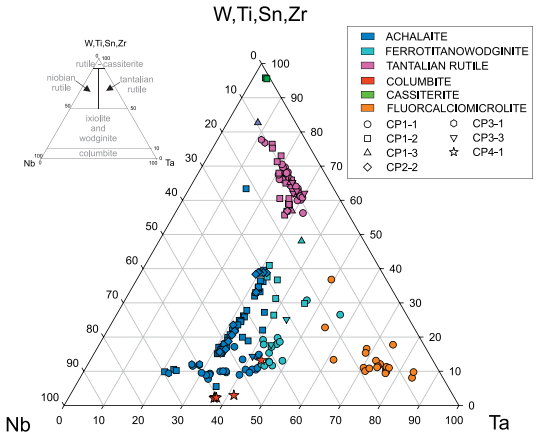

FIG. 6. Compositions of the oxide mineral intergrowths in the La Calandria pegmatite in the Ta–(W + Sn + Ti + Zr)–Nb diagram with the names used in the text. The limit between the compositional fields of the columbite-group minerals and the wodginite-group minerals-ixiolite is taken from Beurlen *et al.* (2007).

groundmass of Ta-rich rutile with ferrotitanowodginite or achalaite inclusions (Fig. 3c).

In massive Ta-rich rutile small fractures filled with fine grains of achalaite/ferrotitanowodginite also occur and, towards the edge of the sample, Ta-rich rutile with variable composition is irregularly intergrown with microlite (Fig. 3d).

In another sample a major domain of achalaite contains thin subparallel cracks filled with small grains of Ta-rich rutile and ferrotitanowodginite. In contact with this domain, Ta-rich rutile occurs with irregular intergrowths of achalaite/ferrotitanowodginite (Fig. 3e). Both domains usually have irregular contacts marked by a rim, probably of ferrotitanowodginite, and are in places partially replaced by fluorcalciomicrolite (Fig. 3f). Figure 3g shows a groundmass of Ta-rich rutile intergrown with subordinate anhedral to subhedral crystals of variable chemical composition, corresponding to either ferrotitanowodginite or achalaite.

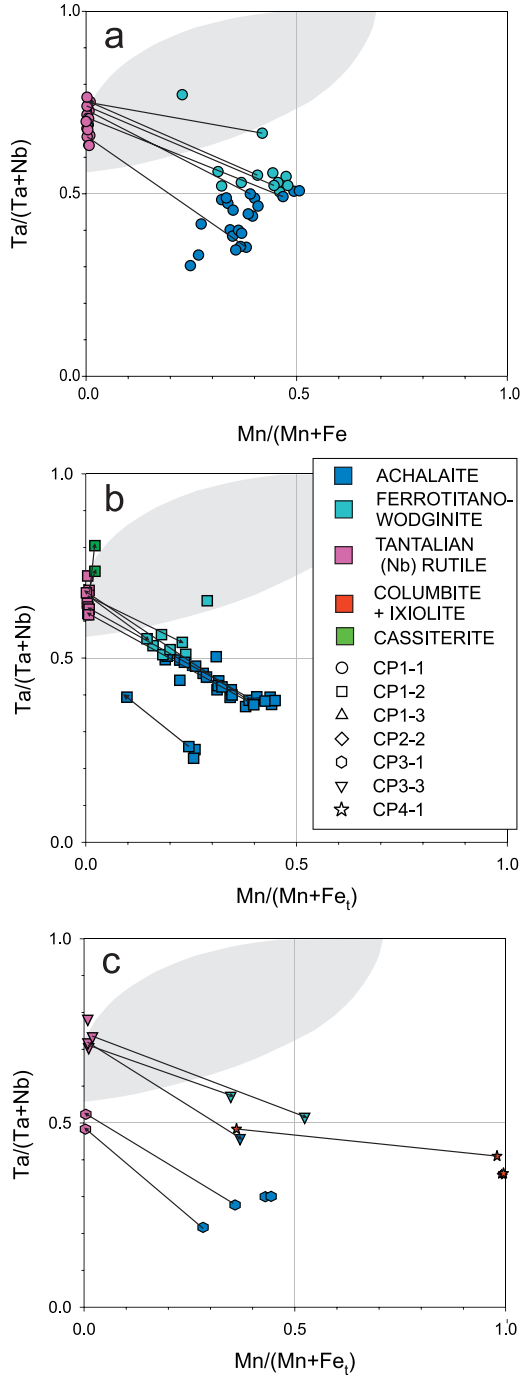

→

FIG. 7. Compositions of pairs of associated achalaite/ferrotitanowodginite, Ta-rich rutile, cassiterite, columbite-(Mn), and ixiolite (CP1-1, CP1-2, CP3-1, CP3-3, and CP4-1) in the columbite quadrilateral. Tielines connect pairs of coexisting minerals; if exsolution is texturally indicated, the composition of the exsolved phase is marked by a arrowhead. The grey area marks the empirical two phase field of orthorhombic + tetragonal phases (from Černý *et al.* 1992).

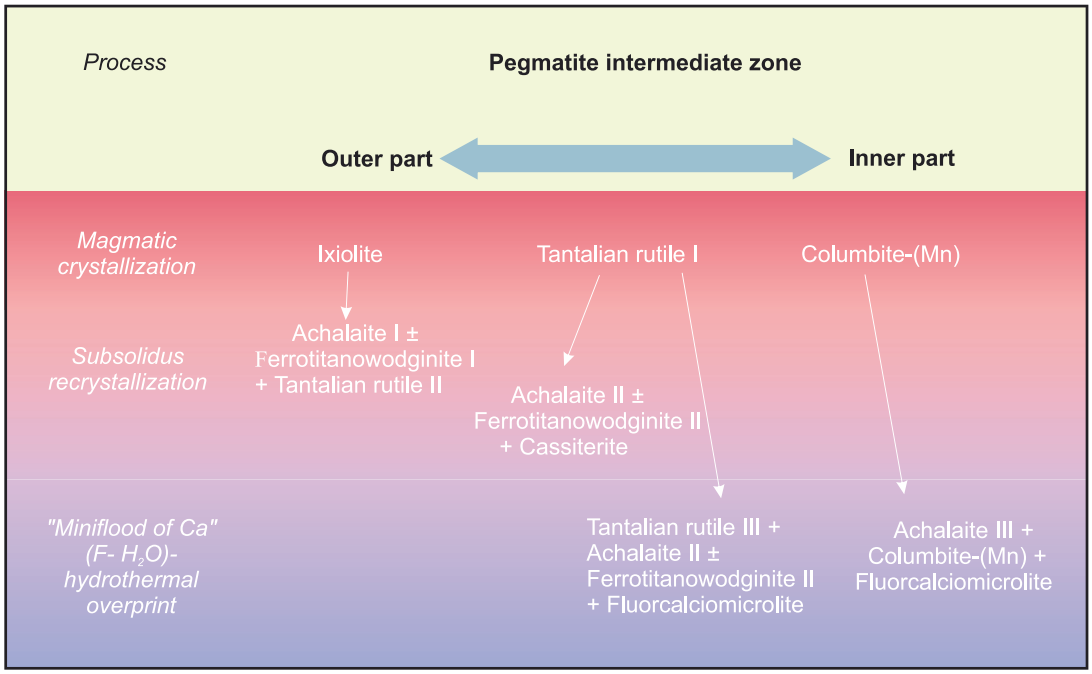

FIG. 8. Schematic diagram connecting the evolution of the intermediate zone of the La Calandria pegmatites and their Nb-Ta-Ti-Sn oxide minerals.

DISCUSSION

The interpretations here are limited by the fine grain size of the assemblage and the difficulties in isolating the separate phases with different chemical compositions for X-ray powder diffraction analysis. Another limitation is the absence of data for Sc, which is possibly present in the Nb-Ta-Ti-Sn oxide minerals, as is suggested by the low totals of some compositions that show increasing contents of calculated Fe^{3+}. Following the approach of Beurlen *et al.* (2007), we set the limit between the fields of the columbite-group minerals and the ixiolite + wodginite-group minerals at 10% (W + Ti + Sn + Zr) *apfu* in the (Mn + Fe_T)–(Nb + Ta)–(W + Ti + Sn + Zr) and Ta–(W + Ti + Sn + Zr)–Nb diagrams (Figs. 5, 6).

With the exception of columbite-(Mn), most of the data lie within the fields of Ta-rich rutile and around the columbite-(Fe)–tantalite-(Fe) border, outside of the fields of ixiolite and wodginite-group minerals of Černý & Ercit (1989), but partially within the columbite-(Fe)–tantalite-(Fe) transition (populated by, *e.g.*, the ferrotitanowodginite of Galliski *et al.* 1999) (Fig. 4). Some partial coincidence exists with compositions of Sc-rich ixiolite plotted in the same type of diagram by Wise *et al.* (1998). The La Calandria compositions correspond to host crystals that have intergrowths of Ta-rich rutile (Fig. 7) or, less frequently, to intergrowths in primary crystals of Ta-rich rutile.

Figure 8 shows a schematic representation of the Nb-Ta-Ti-Sn oxide phases and the processes affecting their crystallization. The textural relationships between all of the phases strongly suggest that the primary magmatic minerals crystallized in different parts of the intermediate zone of the pegmatite, as possibly ixiolite associated with Ta-rich rutile in the outer parts, and columbite-(Mn) in the inner part. Primary ixiolite probably began to crystallize from an undercooled pegmatitic melt that included high contents of minor elements, which produced, reinforced by a fast rate of crystallization, the extremely to totally disordered structure. Tantalum-rich rutile I forms discrete grains that coexist with ixiolite (Fig. 2b). Columbite-(Mn), also considered to be primary, formed at the end of the magmatic crystallization stage in the inner part of intermediate zone of the pegmatite.

Subsolidus cooling conditions followed primary magmatic crystallization, during which the ixiolite–Ta-rich rutile assemblage reached the solvus, and the contents of minor elements in ixiolite exceeded the tolerance of the disordered structure, leading to two consequences: (1) an increase in the structural order of ixiolite that then was transformed, at least in part, to

TABLE 2. SELECTED CHEMICAL COMPOSITIONS OF MINERALS FROM THE LA CALANDRIA GRANITIC PEGMATITE

Phase	RUT	RUT	RUT	RUT	RUT	RUT	RUT	RUT	RUT	RUT	RUT	CGM	CASS
Sample	CP1-1	CP1-1	CP1-1	CP1-1	CP1-2	CP1-2	CP1-2	CP1-3	CP2-2	CP3-1	CP3-3	CP4-1	CP1-2
Point	12	28	39	85	B-04	B-05	B-56	B-58	B-63	B-82	92	96	B-44
Position	incl.	incl.	incl.	exs.	exs.	exs.	coex.	exs.	coex.	exs.	host	host	exs.
WO_3 wt.%	0.38	0.16	0.36	0.05	0.37	0.38	0.46	0.35	0.17	0.12	0.08	0.38	0.01
Ta_2O_5	35.21	43.14	41.13	43.29	32.16	23.95	36.24	38.33	40.66	23.40	44.97	40.45	5.10
Nb_2O_5	10.92	8.63	9.27	8.02	8.95	22.17	13.51	9.45	13.05	12.10	7.32	39.32	0.74
TiO_2	36.98	30.37	32.79	30.68	45.13	36.88	29.71	35.35	27.41	51.67	33.13	0.54	0.91
SnO_2	1.31	1.73	0.96	2.00	1.21	1.66	4.78	2.10	4.05	0.67	1.23	0.35	90.67
ZrO_2	0.00	0.00	0.00	0.00	0.09	0.25	0.17	0.08	0.19	0.03	0.03	0.13	0.13
UO_2	0.00	0.00	0.04	0.00	0.00	0.14	0.00	0.01	0.00	0.00	0.00	0.00	0.01
SiO_2	0.50	0.53	0.37	0.58	0.07	0.34	0.10	0.13	0.30	0.20	0.11	0.59	0.22
Sb_2O_3	0.00	0.00	0.00	0.00	0.00	0.00	0.00	0.00	0.00	0.00	0.00	0.00	0.10
Bi_2O_3	0.04	0.05	0.00	0.00	0.02	0.24	0.00	0.02	0.00	0.00	0.00	0.00	0.01
Fe_2O_3	8.47	7.99	8.84	10.12	8.60	6.41	7.85	8.71	7.42	8.74	7.74	0.26	1.60
FeO	4.68	5.72	5.25	4.61	3.74	5.35	6.02	4.92	6.71	3.06	5.69	0.00	0.00
MnO	0.11	0.06	0.05	0.03	0.09	1.19	0.09	0.05	0.12	0.03	0.09	17.02	0.03
PbO	0.08	0.00	0.09	0.00	0.00	0.00	0.00	0.00	0.00	0.00	0.00	0.06	0.16
CaO	0.11	0.01	0.00	0.02	0.03	0.41	0.02	0.00	0.02	0.03	0.01	0.02	0.18
SrO	0.03	0.00	0.00	0.00	0.03	0.00	0.03	0.00	0.00	0.08	0.06	0.02	0.00
TOTAL	98.82	98.39	99.15	99.40	100.49	99.37	98.98	99.50	100.10	100.13	100.46	99.14	99.87

TABLE 2. CONTINUED.

Phase	RUT	RUT	RUT	RUT	RUT	RUT	RUT	RUT	RUT	RUT	RUT	CGM	CASS
Sample	CP1-1	CP1-1	CP1-1	CP1-1	CP1-2	CP1-2	CP1-2	CP1-3	CP2-2	CP3-1	CP3-3	CP4-1	CP1-2
Point	12	28	39	85	B-04	B-05	B-56	B-58	B-63	B-82	92	96	B-44
Position	incl.	incl.	incl.	exs.	exs.	exs.	coex.	exs.	coex.	exs.	host	host	exs.
W (*apfu*)	0.022	0.010	0.022	0.003	0.020	0.021	0.028	0.020	0.010	0.006	0.005	0.026	0.001
Ta	2.128	2.782	2.581	2.749	1.836	1.387	2.293	2.355	2.605	1.263	2.833	2.953	0.413
Nb	1.097	0.925	0.967	0.847	0.849	2.135	1.421	0.965	1.390	1.086	0.767	4.773	0.100
Ti	6.182	5.417	5.692	5.389	7.126	5.909	5.200	6.009	4.857	7.715	5.774	0.109	0.204
Sn^{4+}	0.116	0.164	0.088	0.186	0.101	0.141	0.443	0.189	0.380	0.053	0.114	0.037	10.753
Zr	0.000	0.000	0.000	0.000	0.009	0.026	0.019	0.009	0.022	0.003	0.003	0.017	0.019
U^{4+}	0.000	0.000	0.002	0.000	0.000	0.007	0.000	0.001	0.000	0.000	0.000	0.000	0.001
Si	0.111	0.126	0.085	0.135	0.015	0.072	0.023	0.029	0.071	0.040	0.025	0.158	0.065
Sb	0.000	0.000	0.000	0.000	0.000	0.000	0.000	0.000	0.000	0.000	0.000	0.000	0.012
Bi	0.002	0.003	0.000	0.000	0.001	0.013	0.000	0.001	0.000	0.000	0.000	0.000	0.001
Fe^{3+}	1.417	1.426	1.534	1.779	1.359	1.027	1.374	1.481	1.315	1.306	1.349	0.052	0.358
Fe^{2+}	0.869	1.134	1.013	0.901	0.656	0.954	1.171	0.930	1.321	0.507	1.102	0.000	0.000
Mn	0.021	0.012	0.010	0.006	0.016	0.215	0.018	0.010	0.024	0.005	0.018	3.871	0.008
Pb	0.005	0.000	0.006	0.000	0.000	0.000	0.000	0.000	0.000	0.000	0.000	0.004	0.013
Ca	0.026	0.003	0.000	0.005	0.007	0.094	0.005	0.000	0.005	0.006	0.002	0.006	0.057
Sr	0.004	0.000	0.000	0.000	0.004	0.000	0.004	0.000	0.000	0.009	0.008	0.003	0.000
TOTAL	12.000	12.002	12.000	12.000	11.999	12.001	11.999	11.999	12.000	11.999	12.000	12.009	12.005
Ta#	0.66	0.75	0.73	0.76	0.68	0.39	0.62	0.71	0.65	0.54	0.79	0.38	0.81
Mn#	0.01	0.00	0.00	0.00	0.01	0.10	0.01	0.00	0.01	0.00	0.01	0.99	0.02
Ti#	0.66	0.59	0.62	0.60	0.73	0.63	0.58	0.64	0.55	0.77	0.62	0.01	0.28

Fe_2O_3 and FeO calculated by charge balancing.
Incl. = inclusion, exs. = exsolution, coex. = coexisting, all related to achalaite/ferrotitanowodginite.

TABLE 3. SELECTED COMPOSITIONS OF FLUORCALCIOMICROLITE FROM THE LA CALADRIA PEGMATITE

Sample	CP1-1	CP1-1	CP1-1	CP1-1	CP1-1	CP1-1	CP1-1	CP1-1	CP1-1	CP1-1	CP1-1	CP1-1	CP1-2	CP1-3	CP3-1
Point	5	6	13	14	15	24	25	37	38	49	50	81	B-03	B-60	B-85
WO_3 (wt.%)	0.50	0.61	0.61	0.31	0.32	0.60	0.23	0.32	0.79	0.27	0.26	0.16	0.16	0.69	0.71
Nb_2O_5	10.07	10.11	9.19	6.65	7.09	9.35	7.27	6.44	8.24	7.36	4.07	3.17	13.88	7.67	11.74
Ta_2O_5	63.15	63.89	54.14	63.85	67.33	64.60	66.75	67.27	62.22	65.10	72.44	66.46	56.67	63.63	47.37
TiO_2	2.75	2.39	13.80	2.52	2.36	2.58	2.25	2.40	3.95	3.06	1.86	2.36	3.87	2.14	6.53
SnO_2	1.22	1.21	1.12	1.14	1.26	1.38	1.18	1.82	2.34	1.29	1.05	0.71	1.00	2.26	0.67
UO_2	0.14	0.66	0.11	0.35	0.32	0.01	0.37	0.58	0.15	0.00	0.71	0.59	0.12	0.24	0.18
SiO_2	0.82	0.23	1.22	2.95	0.47	0.63	0.54	0.42	0.45	0.80	0.07	9.72	2.21	0.17	12.67
Sb_2O_3	0.01	0.00	0.00	0.00	0.03	0.06	0.05	0.00	0.10	0.01	0.00	0.00	0.01	0.04	0.00
Bi_2O_3	0.06	0.10	0.20	0.10	0.06	0.02	0.00	0.00	0.07	0.01	0.08	0.05	0.00	0.04	0.06
CaO	15.99	16.15	10.62	15.72	16.00	16.15	15.99	15.33	15.58	16.32	14.37	10.98	15.91	14.95	13.51
FeO	0.56	0.40	3.73	0.26	0.22	0.16	0.20	0.27	0.56	0.26	0.53	0.17	0.45	0.12	0.21
MnO	0.44	0.27	0.29	0.24	0.16	0.16	0.21	0.08	0.10	0.09	0.11	0.13	0.26	0.07	0.12
PbO	0.00	0.11	0.20	0.07	0.00	0.01	0.06	0.03	0.10	0.03	0.02	0.59	0.18	0.01	0.37
SrO	0.09	0.02	0.00	0.00	0.07	0.02	0.03	0.09	0.10	0.00	0.00	0.00	0.00	0.03	0.07
Na_2O	2.02	1.89	1.71	1.79	1.89	2.20	2.02	2.40	3.20	2.12	2.45	2.30	2.92	3.15	2.84
K_2O	0.01	0.02	0.02	0.01	0.03	0.00	0.01	0.00	0.01	0.03	0.00	0.00	0.00	0.02	0.02
F	2.10	2.19	2.13	2.18	2.32	2.89	1.99	2.76	2.54	1.98	3.23	0.00	2.56	1.98	1.64
O=F	–0.88	–0.92	–0.90	–0.92	–0.98	–1.22	–0.84	–1.16	–1.07	–0.83	–1.36	0.00	–1.08	–0.83	–0.69
TOTAL	99.05	99.33	98.19	97.22	98.95	99.60	98.31	99.05	99.43	97.90	99.89	97.39	99.12	96.38	98.02

TABLE 3. CONTINUED.

Sample	CP1-1	CP1-1	CP1-1	CP1-1	CP1-1	CP1-1	CP1-1	CP1-1	CP1-1	CP1-1	CP1-1	CP1-1	CP1-2	CP1-3	CP3-1
Point	5	6	13	14	15	24	25	37	38	49	50	81	B-03	B-60	B-85
W (*apfu*)	0.010	0.013	0.010	0.006	0.007	0.012	0.005	0.007	0.016	0.006	0.006	0.004	0.003	0.015	0.016
Nb	0.361	0.365	0.267	0.234	0.263	0.337	0.272	0.240	0.296	0.269	0.152	0.129	0.499	0.293	0.447
Ta	1.361	1.388	0.947	1.349	1.504	1.401	1.500	1.509	1.343	1.432	1.632	1.629	1.225	1.460	1.086
Ti	0.164	0.144	0.668	0.147	0.146	0.155	0.140	0.149	0.236	0.186	0.116	0.160	0.231	0.136	0.414
Sn	0.039	0.039	0.029	0.035	0.041	0.044	0.039	0.060	0.074	0.042	0.035	0.026	0.032	0.076	0.023
Si	0.065	0.004	0.079	0.229	0.039	0.050	0.045	0.035	0.036	0.065	0.001	0.195	0.039	0.003	0.238
SUM	2.000	1.953	2.000	2.000	2.000	1.999	2.001	2.000	2.001	2.000	1.942	2.143	2.029	1.983	2.224
U	0.002	0.053	0.002	0.006	0.006	0.000	0.007	0.011	0.003	0.000	0.059	0.053	0.010	0.020	0.015
Sb	0.000	0.000	0.000	0.000	0.001	0.002	0.002	0.000	0.003	0.000	0.000	0.000	0.000	0.001	0.000
Bi	0.001	0.002	0.003	0.002	0.001	0.000	0.000	0.000	0.001	0.000	0.002	0.001	0.000	0.001	0.001
Ca	1.358	1.382	0.732	1.308	1.408	1.380	1.416	1.355	1.325	1.415	1.276	1.060	1.355	1.352	1.220
Fe^{2+}	0.037	0.027	0.201	0.017	0.015	0.011	0.014	0.019	0.037	0.018	0.037	0.013	0.030	0.008	0.015
Mn	0.030	0.018	0.016	0.016	0.011	0.011	0.015	0.006	0.007	0.006	0.008	0.010	0.018	0.005	0.009
Pb	0.000	0.002	0.003	0.001	0.000	0.000	0.001	0.001	0.002	0.001	0.000	0.014	0.004	0.000	0.008
Sr	0.004	0.001	0.000	0.000	0.003	0.001	0.001	0.004	0.005	0.000	0.000	0.000	0.000	0.001	0.003
Na	0.310	0.293	0.213	0.270	0.301	0.340	0.324	0.384	0.492	0.333	0.394	0.402	0.450	0.515	0.464
K	0.001	0.002	0.002	0.001	0.003	0.000	0.001	0.000	0.001	0.003	0.000	0.000	0.000	0.002	0.002
F^{-}	0.526	0.553	0.433	0.536	0.603	0.729	0.520	0.720	0.637	0.507	0.847	0.000	0.644	0.528	0.437
O^{2-}	6.200	6.201	5.469	6.022	6.194	6.094	6.256	6.119	6.151	6.211	5.998	6.572	6.254	6.263	6.529
ΣCAT.	3.743	3.733	3.172	3.621	3.749	3.744	3.782	3.780	3.877	3.776	3.718	3.696	3.896	3.888	3.961
ΣANI.	6.726	6.754	5.902	6.558	6.797	6.823	6.776	6.839	6.788	6.718	6.845	6.572	6.898	6.791	6.966

Atomic contents based on $\Sigma B = 2$. $B = W + Nb + Ta + Ti + Sn + Si$.

partially ordered achalaite I (Nb > Ta at the *C* site) or ferrotitanowodginite I (Nb < Ta at the *C* site), and (2) recrystallization of Ta-rich rutile II (Figs. 2h, 3a). The Ta-rich rutile II and achalaite/ferrotitanowodginite I intergrowths from ixiolite have variable compositions, as shown by the Ta/(Ta + Nb) and Ti/(Ti + Ta + Nb) ratios. The Ta# has ranges of 8.4–30.7% (sample CP1-1), 12.4–23.6% (CP1-2), 23.8–25.8% (CP3-1), and 21.1–25.1% (CP3-3) within individual samples, while the variation in the Ti# is almost double that of the Ta# for these same exsolved samples: 32.7–59.1% (CP1-1), 23.6–76.1% (CP1-2), 67.2–69.6% (CP3-1), and 47.5–67.2% (CP3-3). Under subsolidus cooling conditions, primary Ta-rich rutile I transformed to two phases: ferrotitanowodginite II/achalaite II and cassiterite. This ferrotitanowodginite II/achalaite II formed angular or irregular intergrowths (Fig. 3b) or thin rims between crystals of ferrotitanowodginite I and Ta-rich rutile I.

The process of intergrowths was approximately concurrent with interactions of abundant Ca-F-rich hydrothermal fluids produced during the so-called "miniflood of Ca" process (*cf.* Martin & Devito 2014), which led to fluorcalciomicrolite replacement of achalaite/ferrotitanowodginite I or Ta-rich rutile I under increasing oxygen fugacity. The replacement of Ta-rich rutile I by fluorcalciomicrolite gives Ta-rich rutile III as a by-product, and this generation of Ta-rich rutile III has a higher Ti# than Ta-rich rutile I and achalaite/ferrotitanowodginite II, as shown by the darker color in the BSE image (Fig. 3d).

The secondary modification of primary columbite-(Mn) is simpler; it lies in the peripheral introduction of Fe, Ti, and Sn during the period of hydrothermal overprinting and yields a chemical composition of possibly achalaite III (Fig. 3h).

Conclusions

The crystallization of Nb-Ta-Ti-Sn oxide minerals at La Calandria can be summarized as follows (Fig. 8): a primary, magmatic stage of crystallization produced ixiolite + Ta-rich rutile I + columbite-(Mn) in different parts of the intermediate zone of the pegmatite. Subsolidus fluid-driven dissolution-reprecipitation produced achalaite/ferrotitanowodginite I + Ta-rich rutile II from ixiolite. At the same time, Ta-rich rutile I recrystallized in ferrotitanowodginite/achalaite II + cassiterite. Calcium-F-rich hydrothermal fluids overprinted Ta-rich rutile I, which locally was transformed to Ta-rich rutile III + achalaite/ferrotitanowodginite II + fluorcalciomicrolite. Additionally, these fluids produced peripheral transformation of columbite-(Mn) to possibly achalaite (?) III and widespread distribution of fluorcalciomicrolite in the granular assemblage.

Acknowledgments

The authors are pleased to dedicate this contribution as a tribute to William B. "Skip" Simmons and Karen Webber for their important studies on the mineralogy and geochemistry of granitic pegmatites. This study was made possible by the support of CONICET and FONCYT from Argentina through grants PIP 11220090100857and PICT 22-21637 respectively to M.A. Galliski. National Science and Engineering Research Council of Canada Major Installation and Research Grants to P. Černý and Major Equipment, Research, and Infrastructure grants to F.C. Hawthorne supported the laboratory work at the University of Manitoba. Karen Ferreira kindly helped us by correcting the manuscript. The authors are grateful for the thorough review of the manuscript by Pavel Uher, by the corrections and suggestions of the Associate Editor Pietro Vignola, and for the editorial suggestions of Lee A. Groat.

References

Atencio, D., Andrade, M.B., Christy, A.G., Gieré, R., & Kartashov, P.M. (2010) The pyrochlore supergroup of minerals: nomenclature. *Canadian Mineralogist* **48**, 673–698.

Beurlen, H., Barreto, S.B., Silva, D., Wirth, R., & Olivier P. (2007) Titanian ixiolite – niobian rutile intergrowths from the Borborema Pegmatite Province, northeastern Brazil. *Canadian Mineralogist* **45**, 1367–1387.

Bonalumi, A.A., Sfragulla, J., Martino, R., Zarco, J., Carignano, C., Baldo, E.A., Kraemer, P., Escayola, M., Tauber, A., Cabanillas, A., Juri, E., & Torres, B. (1998) *Hoja geológica 3166-IV Villa Dolores. Provincias de Córdoba y La Rioja. Instituto de Geología y Recursos Minerales*. SEGEMAR – Servicio Geológico Minero Argentino. Programa Nacional de Cartas Geológicas 1:250.000, Versión Preliminar, 122 pp., 1 map, (apendixes: 15 pp.).

Černý, P. & Ercit, T.S. (1989) Mineralogy of niobium and tantalum: crystal chemical relationships, paragenetic aspects and their economic implications. *In* Lanthanides, Tantalum and Niobium (P. Möller, P. Černý, & F. Saupé, eds.). Springer-Verlag, Berlin, Germany (27–79).

Černý, P. & Ercit, T.S. (2005) The classification of granitic pegmatites revisited. *Canadian Mineralogist* **43**, 2005–2026.

Černý, P., Goad, B.E., Hawthorne, F.C., & Chapman, R. (1986) Fractionation trends of the Nb- and Ta-bearing oxide minerals in the Greer Lake pegmatitic granite and its pegmatite aureole, southeastern Manitoba. *American Mineralogist* **71**, 501–517.

Černý, P., Ercit, T.S., & Wise, M.A. (1992) The tantalite-tapiolite gap: natural assemblages *versus* experimental data. *Canadian Mineralogist* **30**, 587–596.

Černý, P., Ercit, T.S., Wise, M.A., Chapman, R., & Buck, H.M. (1998) Compositional, structural and phase relationships in titanian ixiolite and titanian columbite-tantalite. *Canadian Mineralogist* **36**, 547–561.

Chudík, P., Uher, P., Gadas, P., Škoda, R., & Pršek, J. (2011) Niobium-tantalum oxide minerals in the Jezuitské Lesy granitic pegmatite, Bratislava Massif, Slovakia: Ta to Nb and Fe to Mn evolutionary trends in a narrow Be, Cs-rich and Li, B-poor dike. *Mineralogy and Petrology* **102(1–4)**, 15–27.

Demange, M., Álvarez, J.O., López, L., & Zarco, J.J. (1996) The Achala batholith (Córdoba, Argentina): a composite intrusion made of five independent magmatic suites. Magmatic evolution and deuteric alteration. *Journal of South American Earth Sciences* **9(1–2)**, 11–25.

Dorais, M.J., Lira, R., Chen, Y., & Tingey, D. (1997) Origin of biotite- apatite-rich enclaves, Achala batholith, Argentina. *Contributions to Mineralogy and Petrology* **130**, 31–46.

Ercit, T.S. (1994) The geochemistry and crystal chemistry of columbite-group minerals from granitic pegmatites, southwestern Grenville Province, Canadian Shield. *Canadian Mineralogist* **32**, 421–438.

Franchini, M., Lira, R., & Sfragulla, J. (1998) El skarn Cañada del Puerto (31° 25′ LS; 64° 54′ LO), provincia de Córdoba: otro ejemplo de metasomatismo caracterizado por fluidos ricos en agua, hidrógeno y flúor. *Revista Asociación Geológica Argentina* **53(2)**, 247–260.

Gaido, M.F., Zarco, J.J., Miró, R.C., Sapp, M., Gamba, M.T., & López, H. (2005). Hoja geológica 3166-30: Los Gigantes, provincia de Córdoba, 1:100.000. Servicio Geológico Minero Argentino, Instituto de Geología y Recursos Minerales, Boletín 299, Buenos Aires, Argentina, 126 pp.

Galliski, M.A., Černý, P., Márquez-Zavalía, M.F., & Chapman, R. (1999) Ferrotitanowodginite, $Fe^{2+}TiTa_2O_8$, a new mineral of the wodginite group from the San Elías pegmatite, San Luis, Argentina. *American Mineralogist* **84**, 773–777.

Galliski, M.A., Márquez-Zavalía, M.F., Černý, P., Martínez, V., & Chapman, R. (2008) The Ta-Nb-Sn-Ti oxide-mineral paragenesis at La Viquita, a spodumene-bearing rare-element granitic pegmatite from San Luis, Argentina. *Canadian Mineralogist* **47(2)**, 379–393.

Galliski, M.A., Márquez-Zavalía, M.F., Černý, P., Lira, R., Colombo, F., Roberts, A., & Berndhart, H.J. (2016) Achalaite, $Fe^{2+}TiNb_2O_8$, a new member of the wodginite-group minerals from a granitic pegmatite of Córdoba Argentina. *Canadian Mineralogist* **54** (this volume).

Gay, H.D. & Lira, R. (1984) Presencia de topacio en la provincia de Córdoba. Yacencia, mineralogía y paragénesis en Tanti y Cañada del Puerto. *Revista Asociación Argentina Mineralogía, Petrología y Sedimentología* **15(3–4)**, 62–66.

Gordillo, C.E. (1979) Observaciones sobre la petrología de las rocas cordieríticas de la Sierra de Córdoba. *Boletín Academia Nacional de Ciencias* **53(1–2)**, 3–44. Córdoba.

Hanson, S.H., Simmons, W.B., Jr., & Falster, A.U. (1998) Nb-Ta-Ti oxides in granitic pegmatites from the Topsham pegmatite district, southern Maine. *Canadian Mineralogist* **36**, 601–608.

Kontak, D.J. (2006) Nature and origin of an LCT-suite pegmatite with late-stage sodium enrichment, Brazil Lake, Yarmouth County, Nova Scotia. I. Geological setting and petrology. *Canadian Mineralogist* **44**, 563–598.

Lira, R. & Kirschbaum, A.M. (1990) Geochemical evolution of granites from the Achala batholith of the Sierras Pampeanas, Argentina. *In* Plutonism from Antarctica to Alaska, Boulder, Colorado (S.M. Kay & C.W. Rapela, eds.). *Geological Society of America, Special Paper* **241**, 67–76.

Lucero Michaut, H.N. & Daziano, C.O. (1984) *Un gran stock metagábricopreplutónico y su cortejo de gabros metamórficos asociados*. 9th Congreso Geológico Argentino, Cañada del Puerto - Sierras de Córdoba, Actas II, San Carlos de Bariloche, 231–242.

Lumpkin, G.R. (1998) Composition and structural state of columbite-tantalite from the Harding pegmatite, Taos County, New Mexico. *Canadian Mineralogist* **36**, 585–599.

Martin, R. & Devito, C. (2014) The late-stage miniflood of Ca in granitic pegmatites: and open system acid-reflux model involving plagioclase in the exocontact. *Canadian Mineralogist* **52**, 165–181.

Novák, M. & Černý, P. (1998) Niobium-tantalum oxide minerals from complex granitic pegmatites in the Moldanubicum, Czech Republic: primary *versus* secondary compositional trends. *Canadian Mineralogist* **36**, 659–672.

Novák, M., Černý, P., & Uher, P. (2003) Extreme variation and apparent reversal of Nb-Ta fractionation in columbite-group minerals from the Scheibengraben beryl-columbite granitic pegmatite, Maršíkov, Czech Republic. *European Journal of Mineralogy* **15(3)**, 565–574.

Pouchou, J.L. & Pichoir, F. (1985) "PAP" ($\phi\rho Z$) correction procedure for improved quantitative microanalysis. *In* Microbeam Analysis (J.T. Armstrong, ed.). San Francisco Press, San Francisco, California, United States (104–106).

Spilde, M.N. & Shearer, C.K. (1992) A comparison of tantalum-niobium oxide assemblages in two mineralogically distinct rare-element granitic pegmatites, Black Hills, South Dakota. *Canadian Mineralogist* **30**, 719–737.

Tindle, A.G. & Breaks, F.W. (1998) Oxide minerals of the Separation Rapids rare-element granitic pegmatite group, northwestern Ontario. *Canadian Mineralogist* **36**, 609–635.

Tindle, A.G., Breaks, F.W., & Webb, P.C. (1998) Wodginite-group minerals from the Separation Rapids rare-element granitic pegmatite group, northwestern Ontario. *Canadian Mineralogist* **36**, 637–658

Uher, P., Černý, P., Chapman, R., Határ, J., & Miko, O. (1998a) Evolution of Nb,Ta-oxide minerals in the Prašivá granitic pegmatite, Slovakia. I. Primary Fe, Ti-rich assemblage. *Canadian Mineralogist* **36**, 525–534.

Uher, P., Černý, P., Chapman, R., Határ, J., & Miko, O. (1998b) Evolution of Nb,Ta-oxide minerals in the Prašivá granitic pegmatite, Slovakia. II. External hydrothermal Pb, Sb overprint. *Canadian Mineralogist* **36**, 535–545.

Van Lichtervelde, M., Salvi, S., Beziat, D., & Linnen, R. (2007) Textural features and chemical evolution in tantalum oxides: magmatic versus hydrothermal origins for Ta mineralization in the Tanco Lower pegmatite, Manitoba, Canada. *Economic Geology* **102**, 257–276.

Wise, M.A., Černý, P., & Falster, A.U. (1998) Scandium substitution in columbite-group minerals and ixiolite. *Canadian Mineralogist* **36**, 673–680.

Zhang, A.C., Wang, R.C., Hu, H., Zhang, H., Zhu, J.C., & Chen, X.M. (2004) Chemical evolution of Nb-Ta oxides and zircon from the Koktokay N° 3 granitic pegmatite, Altai, northwestern China. *Mineralogical Magazine* **68**, 739–756.

Received October 7, 2015. Revised manuscript accepted June 4, 2016.